

# A Symmetry-Based Generative Model for Shape

Nhon H. Trinh  
Brown University  
Providence, RI 02912, USA  
ntrinh@lems.brown.edu

Benjamin B. Kimia  
Brown University  
Providence, RI 02912, USA  
kimia@lems.brown.edu

## Abstract

We propose a novel generative language for shape that is based on the shock graph: given a shock graph topology, we explore constraints on the geometry and dynamics of the shock graph branches at each point required to generate a valid shape, *i.e.*, with no self-intersection, cusps, or crossovers. We model the shape boundary as a piecewise smooth circular arc spline, which is dense in the space of piecewise smooth curves. Using this model we derive an independent set of parameters which generate a variety of shapes and satisfy the reconstruction constraints. We show simple examples of using this generative model as an active deformable shape and for morphing between two shapes. The results illustrate that it is possible to generate any generic shape with relatively few parameters, further reduced if prior knowledge of shape is available.

## 1. Introduction

Representation of shape is key in recognition, segmentation, tracking, and other visual tasks. In one class of representations, the mapping of the intrinsically high-dimensional shape space to a lower-dimensional representation is not explicitly invertible, *e.g.*, encoding by shape invariants [18] or shape context [3]. In a second class of representations, an explicit reconstruction of the equivalence class of shapes is possible [22, 12, 20]. We refer to these as *generative models for shape*. While the first class of representations are quite sufficient in some applications, *e.g.*, recognition from shape boundary, generative representations are required in others. For example, in model-based segmentation, prior knowledge is encoded in the representation, thus requiring an understanding of the class of shapes each representation maps to, so that restrictions on the representation can be mapped to restrictions of shape to a particular class of forms. Similarly, in tracking objects in a video sequence the observed shape in previous frames constitutes prior knowledge for the subsequent frames. In statistical shape analysis, characterization of the notion of

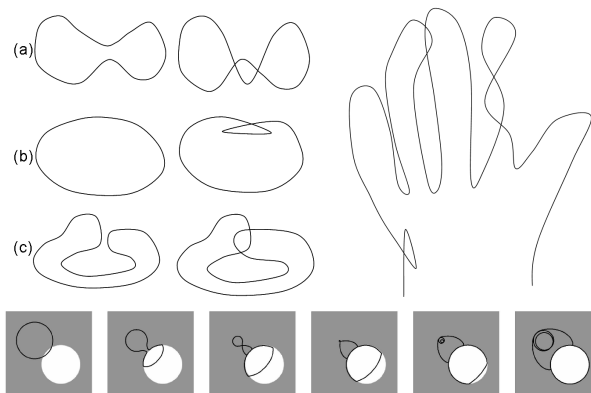


Figure 1. (Top) Generative models of shape need to avoid generating invalid or “illegal” shapes, *i.e.*, with self-intersection, swallowtails, unwanted topology changes, *etc.* (Bottom) From [10] A parametric active contour, or snake, can self-intersect as it deforms to capture the shape of interest in an image.

shape average and shape variance are not necessarily meaningful in the representation space, and the inverse mapping between the representation and the generated shape is necessary to effect proper averaging in the shape space. In interactive shape modeling, the “editing” of shapes, such as bending, stretching, thinning, *etc.*, needs to be translated into a transformation on the shape representation, requiring an explicit inverse mapping from the transformed representation [11]. In generating shape morphing sequences, the representations of the “initial” and “final” shapes are interpolated, the results of which are used to generate shapes in the sequence, using the representation to shape mapping [1].

Generative models of shape face challenges not experienced by non-generative models. First, a given representation must generate a “legal” shape, a member in good standing, *i.e.*, without self-intersections, swallowtails, with valid topology, Figure 1. Second, the model has to be capable of generating a comprehensive and *complete* variety of shapes, approximated to the desired level of accuracy. Indeed some of the existing shape models may leave out big chunks of the shape space, *e.g.*, active shape models generate shapes only

for the classes learnt [6]. Third, a generative model needs to balance *expressiveness* of the model with its *dimensionality*. The challenge, given the extremely high-dimensional shape space, is to capture the essential variations in shape while ignoring the irrelevant ones. While free-form models, *e.g.*, “snakes” and its level-set counterpart, generate a wide variety of shapes, they are high-dimensional. In contrast, parametric models such as superquadrics or Fourier models restrict the dimensionality of the model, but this is at the expense of discarding large chunks of the shape space.

Previous generative models can be organized into four classes. First, active contours or “snakes” [14] and their level-set counterpart [17] are sampled contours and sampled distance transform of contours, respectively, and are perhaps the most popular segmentation tool. The contour-based representation can experience problems illustrated in Figure 1, while the level-set counterpart avoids these, but its often-praised flexibility of topological change is not easy to control [10]. The very high-dimensional nature of the representation affords maximal expressiveness, but this requires optimization by local (gradient descent) methods, facing the dreaded local minimum problem. To resolve this problem, some approaches have restricted the shape of these active models by using prior knowledge [15, 7]. However accurate learning of the prior from sample shapes is a difficult task due to the high-dimensionality of the model.

A second class of methods model the variability of shape by deformations from a known prototype or template/atlas. In this approach, the template shape can be modeled as an unorganized point cloud (known landmarks) [5, 6], by a contour, or by other shape representations. The deformation is also modeled in a variety of ways, either as independent variation of each landmark modeled by a Gaussian, as pairwise interaction of variation using PCA [6], or by imposing a model of deformation for the extrinsic canvas on which the landmarks or template are painted [5, 4, 9, 12]. With the use of unorganized point clouds or contours as shape representation illegal shapes can arise during the above deformations, except for the extremely high-dimensional diffeomorphism approach [9].

A third class of methods model shape as parametric deformable primitives such as superquadrics [23], or Fourier models [22]. The use of these primitives is attractive in that the representation is low-dimensional, but it is also severely limited in its expressiveness. Modeling shapes as unions of primitive, as used in the Thingworld [19], is very appealing as it increases the range of shapes which can be modeled without much additional cost, but the process of bringing primitives together is not well-defined. A key contribution of our work is that the connectivity of the various components of shape is represented in the topology of the medial axis, while also satisfying the boundary condition of how components are brought together.

A fourth class of methods, initially used by Yuille *et al* [26], are graph-based representation of shape, *e.g.*, the hand model of [24] or the body graph of [2]. The use of a graph is desirable in that it models the spatial relationship of the components. The shape representations can be based on nodes sampling the interior of shape [24], manually designed graphs connecting landmarks, contours [29], or the symmetry/medial axis [20, 13]. The effectiveness of these methods has been demonstrated in applications involving class-specific shape, *e.g.*, when shapes are limited to hands, faces, bodies, and anatomical structures such as liver, kidney, and blood vessels. In this paper we develop a framework for generating a *general class* of shapes.

Pizer [20] and Joshi [13] pioneer the use of a predetermined and *fixed topology skeleton* to model a population of anatomic structures in 3D images. The representation, referred to as m-rep, is a discrete sampling of the medial axis and its local geometry. Due to its discrete nature, continuous interpolation can fail to generate valid shapes. A continuous function representation of the medial geometry and the radius field was explored in Yushkevich *et al* [27] and improved in [28], which modeled a medial axis branch by a Poisson PDE with a non-linear boundary condition in order to solve the boundary constraints in bringing together several branches. In the process, the medial axis branches are described on a common parameter domain, allowing for comparison across instances. While this is a significant progress that allows for statistical shape comparison, the problem of shape synthesis from a medial axis of arbitrary topology remains unsolved. The contribution of this paper is to solve this problem for 2D shape and to pioneer a new generative model for shape synthesis. We have developed a significant portion of the theory required for the use of this model in applications, and illustrate its potential through several examples.

The paper is organized as follows. In Section 2 we review the representation of shape by the shock graph, a variant of the medial axis. Each segment (link) of the shock graph generates a fragment of the shape (various colored regions in Figure 4c). We formulate the space of all shape fragments for a given shock segment in Section 3 and examine constraints imposed in putting adjacent shape fragments together in Section 4. In Section 5, we take this a step further and put all shape fragments for any shock graph together to generate a complete shape. This concludes the presentation of the theoretical framework for generating *legal* shapes for a given shock graph topology. This is the main contribution of this paper. In Section 6, we illustrate the *potential* of this approach by showing the variety of shapes generated for a hand example, by highlighting how it can be used as an active deformable model, and by showing a morphing example. These examples are not intended to validate a complete application of the theory but rather to

illustrate its potential.

## 2. The Medial Axis and the Shock Graph

Two significant questions underly the generic synthesis of shapes from a given medial axis topology. First, what is the valid domain of variation of geometry and radius for any given medial axis branch? Second, what are the constraints as branches come together so that the reconstructed shape segments come together smoothly? Together, the answers to these questions should identify the free variables that remain for generating shapes for a given medial axis topology.

The medial axis is not sufficiently discriminative as an indicator of the qualitative shape as shown in Figure 2, *i.e.*, given a medial axis topology a much wider variety of shape are possible. Since we would like the given topology to qualitatively describe the shape we model shapes based on a variant of the medial axis, the shock graph [8], which significantly limits the variation to qualitatively similar forms. The shock graph is a refinement of the medial axis by treating the radius as time and augmenting the geometry of the medial axis by the dynamics of monotonically flowing shocks, Figure 2.

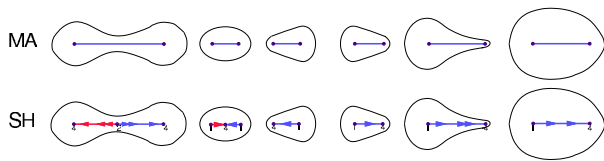


Figure 2. From [8], the advantage of the shock graph over medial axis is its qualitative description of the boundary: given a medial axis segment any of the six shapes in the top row can occur, while a shock graph segment (a monotonically flowing subsegment of the medial axis) qualitatively represents one type of shape.

To generate shapes from a shock graph topology, the first and foremost issue is to find a low-dimensional space from which shock geometry and shock dynamics can be selected for each shock branch such that the reconstructed boundaries of neighboring shock fragments match. Unfortunately, such a space is difficult to express directly in the shock domain for several reasons. First, approximating the shock geometry and dynamics independently does not guarantee that a valid shape, *i.e.* one without intersections, can be constructed, Figure 3. Second, it is not clear that such a reconstruction would sample the space of shapes densely and uniformly, *i.e.*, some shapes may not be reached. Third, it is not clear how the constraints of matching adjacent shape fragments can be satisfied, if at all. Thus, we focus on expressing the shock geometry and dynamics as inherited directly from models of the shape boundary.

We select a fairly generic space of boundaries, namely, **Piecewise Circular Arc Splines (PCAS)**, which we de-

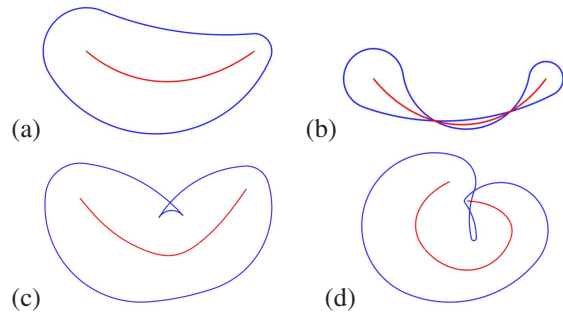


Figure 3. (a) A simple shape and its shock graph. Invalid reconstruction can result due to, for example, (b) intersection of boundaries of the two sides, (c) formation of a “swallow tail”, or (d) non-local intersection

fine as an ordered collection of circular arc segments with matching end-points and end-point tangents, Figure 4(a). The set of PCAS densely samples the set of piecewise smooth curves in the sense that any piecewise smooth curve can be approximated to any degree of accuracy by a PCAS [25]. This renders the space of shock graphs of piecewise circular splines a suitable platform to generate shapes from their shock graphs. Note that while the space of polylines is also a dense sampling of the space of piecewise smooth curves, polylines are only  $C^0$ , in contrast to piecewise circular splines which can be  $C^1$ , if needed. Figures 4(b,c) show the fragments of a shape corresponding to shock segments of the boundary as modeled by a PCAS.

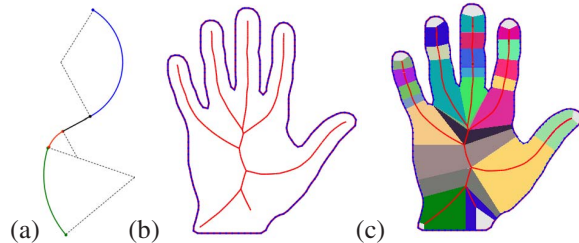


Figure 4. (a) A piecewise circular spline (PCAS): the end points and end tangents of the circular arcs match. Straight line segments are allowed. (b) A hand shape approximated by a piecewise circular spline (black) and its shock graph (red). (c) The shock fragments for this approximation.

The medial axis graph topology can *generally* be discussed as consisting of two types of nodes [8]: (i)  $A_3$  nodes, which are the end points of the medial axis and arise from curvature extrema, and (ii)  $A_1^3$  nodes, which are the intersection of three branches of the medial axis<sup>1</sup>. The nodes are connected by links which are curves of (iii)  $A_1^2$  nodes, which are centers of maximally inscribed bi-tangent circles. Aside from these generic types, we are also interested in types arising when considering a one-parameter deformation sequence, namely, (iv)  $A_1^4$  points when four branches

<sup>1</sup>The  $A_k^n$  terminology indicates medial points with  $k$ -fold order of contact with the medial circle at  $n$  distinct points.

come together, and (v)  $A_1 A_3$  points which are the beginning of a protrusion sequence. Finally, we must also consider nodes which are non-generic in the family of piecewise smooth shapes, but are generic in the family of piecewise circular arcs, namely, (vi)  $A_\infty$  points, which are centers of boundary circular arcs.

A shock graph, inheriting properties of a medial axis, generally has six types of shocks [8]: (i)  $A_3$  as before, (ii)  $A_1^2 - 2$  are  $A_1^2$  points with non-vanishing flow (gradient of the radius function), (iii)  $A_1^2 - 2$  are  $A_1^2$  points which are sources of flow, (iv)  $A_1^4 - 4$  are  $A_1^2$  points which are sinks of flow, (v)  $A_1^3 - 4$  are  $A_1^3$  points with all branches flowing into the  $A_1^3$ , and (vi)  $A_1^3 - 2$  are  $A_1^3$  points with two inward and one outward flow. No other combinations are generally possible. The shock graph is constructed with  $A_1^2$  segments linking the remaining types as nodes. A *shape fragment* is the set of all points of the shape that are in the influence zone of a given shock segment, as color-coded in Figure 4(c). These fragments are the basic atomic elements of our language for generating shapes.

The reconstruction process from each shock segment is described in [8]: Let  $(T, N)$  be the tangent and normal to the medial axis  $\gamma$ , and let  $r$  be the radius of the bi-tangent circle. Let  $N^\pm$  be the vectors orthogonal to the shape boundary at each shock point with “+” and “-” indicating the left and right sides with respect to  $T$ , respectively and let  $\phi = \angle(T, N^+)$ . The reconstructed boundaries  $\gamma^\pm$  are computed as  $\gamma^\pm = \gamma + r \cos \phi T \pm r \sin \phi N$ , with  $N^\pm = -\cos \phi T \mp \sin \phi N$ .

### 3. Shape Fragments from Shocks

Our approach to formulating the space of all shapes that can legitimately arise from a given shock graph, *e.g.*, as shown in Figure 4(a), is to first examine all shapes that can arise from each individual shock segment without paying attention to whether this fragment of shape matches the adjacent fragments. Two types of fragments generically arise: the generic  $A_1^2$  fragments and the  $A_\infty$  fragments, which arise from the quenching of a circular arc at its center and forming  $A_\infty$  nodes. The  $A_\infty$  nodes are degenerate in the space of piecewise smooth curves, but are generic in the space of PCAS.

**$A_1^2$ -fragments:** Figure 5 shows the boundary reconstruction from any portion of an  $A_1^2 - 1$  shock segment. We restrict each reconstructed boundary,  $EF$  and  $GH$ , to be a single circular arc. In this way the entire  $A_1^2$  shock segment can reconstruct a circular arc spline. Denote the tangent to the medial axis at  $A$  and  $B$  as  $T_A$  and  $T_B$ . Let  $\alpha_A = \angle(\overrightarrow{AB}, T_A)$ ,  $\alpha_B = \angle(\overrightarrow{BA}, T_B)$ ,  $\phi_A = \angle(T_A, N_A^+)$ , and  $\phi_B = \angle(T_B, N_B^+)$ .

**Proposition 1.** For an  $A_1^2$  shape fragment with notations as

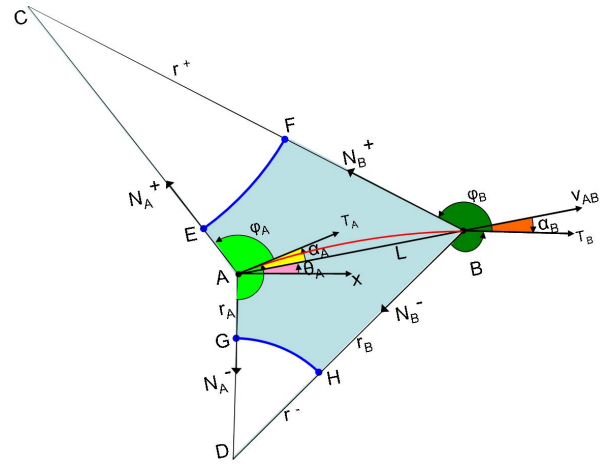


Figure 5. Notations related to a shock segment  $AB$ , shown in red, and the corresponding shape fragment, shaded in blue and bounded by  $AGHBF E$ .

in Figure 5, we have

$$\begin{cases} r_A - r_B = AB \cdot \frac{\cos\left(\frac{\phi_B + \alpha_B}{2} + \frac{\phi_A + \alpha_A}{2}\right)}{\cos\left(\frac{\phi_B + \alpha_B}{2} - \frac{\phi_A + \alpha_A}{2}\right)}, \\ \frac{\sin \alpha_A}{\sin \phi_A} = -\frac{\sin \alpha_B}{\sin \phi_B}. \end{cases} \quad (1)$$

Based on this proposition representing  $\phi_A$ ,  $\phi_B$ , and the ratio  $m = \frac{\sin \alpha_A}{\sin \phi_A}$ , referred to as the *m-factor*, is sufficient to compute  $\alpha_A$  and  $\alpha_B$ . In addition if we know  $r_A$  and the chord length,  $L = |AB|$ , then we can compute  $r_B$ . Since scaling the shape linearly affects  $L$  and  $r_A$  in the same way we define a size attribute  $\lambda$  and angle  $\eta$  to describe the relative magnitude of  $L$  and  $r_A$ :  $\lambda_A = \sqrt{r_A^2 + L^2}$  and  $(\cos \eta_A, \sin \eta_A) = \frac{(L, r_A)}{\sqrt{r_A^2 + L^2}}$ , or equivalently,  $L = \lambda_A \cos \eta_A$  and  $r_A = \lambda_A \sin \eta_A$ .

**Definition 1.** ( $A_1^2$  fragment parameter set)

The extrinsic parameters  $(x_A, y_A, \theta_A, \lambda_A)$ , and the intrinsic parameters  $(\phi_A, \phi_B, m, \eta_A)$  constitute the  $A_1^2$  fragment parameter set with respect to shock node  $A$ , Figure 6:

$$\chi_{AB} = \{(x_A, y_A, \theta_A, \lambda_A), (\phi_A, \phi_B, m_A), \eta_A\}, \quad (2)$$

where  $(x_A, y_A)$  is the location of the node  $A$ ,  $\theta_A$  is the orientation of the shock chord,  $\theta_A = \angle(x\text{-axis}, \overrightarrow{AB})$ ,  $\phi_A = \angle(T_A, N_A^+)$ ,  $\phi_B = \angle(T_B, N_B^+)$ ,  $m$  is the *m-factor* defined as  $m = \frac{\sin \alpha_A}{\sin \phi_A}$  with  $\alpha_A = \angle(\overrightarrow{AB}, T_A)$ , and  $\lambda_A$  and  $\eta_A$  are as described above.

**Proposition 2.** The  $A_1^2$  fragment parameter set is complete and minimal: Two  $A_1^2$  fragments are identical up to a similarity transform if and only if their  $\phi_A$ ,  $\phi_B$ ,  $m_A$ , and  $\eta_A$  are identical. In addition, if  $\lambda_A$  are identical then the two shapes are identical and vice versa.

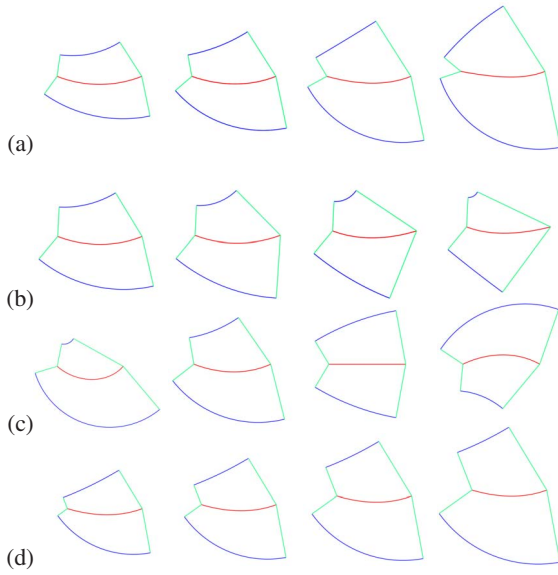


Figure 6. The effect of variations in the  $A_1^2$  fragment set on the reconstructed fragment is illustrated. Changes in  $x_A$ ,  $y_A$ ,  $\theta_A$ , and  $\lambda_A$  produce translation, rotation, and scaling, and are not shown here. The effect of changing  $\phi_A$ ,  $\phi_B$ ,  $m_A$ , and  $\eta_A$  in isolation is illustrated in (a-d), respectively. Note that  $\phi_A$  and  $\phi_B$  capture the shock dynamics, indicating the rate of change of the radius function, or how fast the fragment is getting “thinner” or “fatter”, while  $m_A$  is effectively a bending parameter and  $\eta_A$  decides how “fat” or “thin” the fragment is.

The following proposition establishes the constraints on the free parameters so that the reconstructed boundary of an  $A_1^2$  fragment is free of local intersections, e.g., Figure 3(a-c).

**Proposition 3. (Legality constraints)**

(a) For an  $A_1^2$  shape fragment, at least one of the two boundary circular arcs is less than half a circle and  $(\phi_A - \frac{\pi}{2})(\phi_B - \frac{\pi}{2}) > 0$ .

(b) The necessary conditions for an  $A_1^2$  parameter set  $\chi_{AB} = \{(x_A, y_A, \theta_A, \lambda_A), (\phi_A, \phi_B, m_A), \eta_A\}$  to give rise to a valid  $A_1^2$  fragment (no self-intersections) are: (i)  $0 < \phi_A < \pi$ ,  $0 < \phi_B < \pi$ , and  $(\phi_A - \frac{\pi}{2})(\phi_B - \frac{\pi}{2}) > 0$ , (ii)  $0 < L$ , (iii)  $|m_A \sin \phi_A| < 1$  and  $|m_A \sin \phi_B| < 1$ , and (iv)  $0 < r_A < \min\left(L \frac{\sin(\phi_B + \alpha_B)}{\sin((\phi_B + \alpha_B) - (\phi_A + \alpha_A))}, L \frac{\sin(\phi_B - \alpha_B)}{\sin((\phi_B - \alpha_B) - (\phi_A - \alpha_A))}\right)$  where  $\alpha_A, \alpha_B \in (\frac{\pi}{2}, \frac{\pi}{2})$  such that  $\sin \alpha_A = m_A \sin \phi_A$  and  $\sin \alpha_B = -m_A \sin \phi_B$ .

**Definition 2. ( $A_\infty$  fragment parameter set)**

The extrinsic parameters,  $(x_A, y_A, \theta_A, r_A)$ , and the intrinsic parameter,  $\phi_A$ , constitute the  $A_\infty$  fragment parameter set, Figure 7:

$$\chi_{A_\infty} = \{(x_A, y_A, \theta_A, r_A), \phi_A\}, \quad (3)$$

where  $(x_A, y_A)$  is the location of the node A,  $\theta_A$  is the

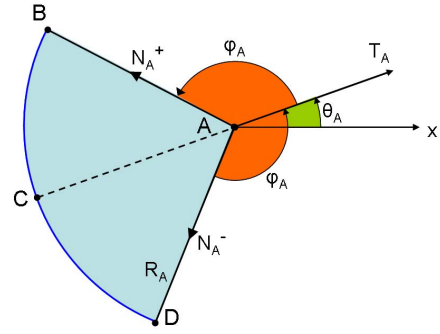


Figure 7. An  $A_\infty$  fragment (shaded in blue) and the related parameters. The only intrinsic variation of an  $A_\infty$  fragment is with the parameter  $\frac{\pi}{2} \leq \phi_A < \pi$ .  $x_A, y_A, \theta_A, r_A$  translate, rotate, and scale the fragment respectively.

direction the shock tangent,  $\theta_A = \angle(x\text{-axis}, T_A)$ ,  $\phi_A = \angle(T_A, N_A^+)$ , and  $r_A$  is the radius of the circular arc.

**Proposition 4.** The  $A_\infty$  fragment is complete and minimal: Two  $A_\infty$  fragments with matching  $\phi_A$  are identical up to a similarity transform. In addition, if  $r_A$  also match then the two fragments are identical and vice versa.

The range of these parameters is  $(x_A, y_A) \in R^2$ ,  $\theta_A \in [0, 2\pi)$ ,  $r_A \in (0, \infty)$ , and  $\phi_A \in (0, \pi)$ . It is interesting that one can think of the  $A_\infty$  fragment as the limit of an  $A_1^2$  fragment where  $\eta_A \rightarrow \frac{\pi}{2}$ ,  $\phi_B \rightarrow \pi$ , and  $m_A \rightarrow 0$ .

## 4. Putting pairs of shock fragments together

In the previous section we studied how each individual shock fragment can be constructed and varied in a symmetric manner via a minimal (non-redundant) set of extrinsic and intrinsic parameters. Clearly, putting these fragments together requires that adjacent fragments match in the sense that the corresponding pairs of contours must come together and their tangents must align. These constraints are enumerated below:

**I.  $A_1^2$ - $A_1^2$  fragments:** Let the fragment  $\chi_{AB} = \{(x_A, y_A, \theta_A, \lambda_A), (\phi_A, \phi_B, m_A), \eta_A\}$  match with  $\chi_{\overline{A}\overline{B}} = \{(x_{\overline{A}}, y_{\overline{A}}, \theta_{\overline{A}}, \lambda_{\overline{A}}), (\phi_{\overline{A}}, \phi_{\overline{B}}, m_{\overline{A}}), \eta_{\overline{A}}\}$  end to end, i.e.,  $B \equiv \overline{A}$ . We have five constraints, Figure 8(a), (i)  $x_B = x_{\overline{A}}$  (ii)  $y_B = y_{\overline{A}}$ , (iii)  $r_B = r_{\overline{A}}$ , (iv)  $\theta_B + \alpha_B = \theta_{\overline{A}} + \alpha_{\overline{A}}$ , (v)  $\phi_B = \phi_{\overline{A}}$ . Thus a pair of matching  $A_1^2$ - $A_1^2$  fragments have  $8 + 8 - 5 = 11$  free variables.

**II.  $A_1^2$ - $A_\infty$  fragments:** Let the fragment  $\chi_{A_\infty} = \{(x_A, y_A, \theta_A, r_A), \phi_A\}$  match with  $\chi_{\overline{A}\overline{B}} = \{(x_{\overline{A}}, y_{\overline{A}}, \theta_{\overline{A}}, \lambda_{\overline{A}}), (\phi_{\overline{A}}, \phi_{\overline{B}}, m_{\overline{A}}), \eta_{\overline{A}}\}$ . Then, we have again five constraints, Figure 8(b), (i)  $x_A = x_{\overline{A}}$ , (ii)  $y_A = y_{\overline{A}}$ , (iii)  $r_A = r_{\overline{A}}$ , (iv)  $\theta_A = \theta_{\overline{A}} + \alpha_{\overline{A}}$ , (v)  $\phi_A = \phi_{\overline{A}}$ . Thus, the number of constraints fully consumes the degree of freedom of the  $A_\infty$  fragment.

**III.  $A_1^3$  - 4 fragments (three  $A_1^2$  fragments at an  $A_1^3$  - 4**

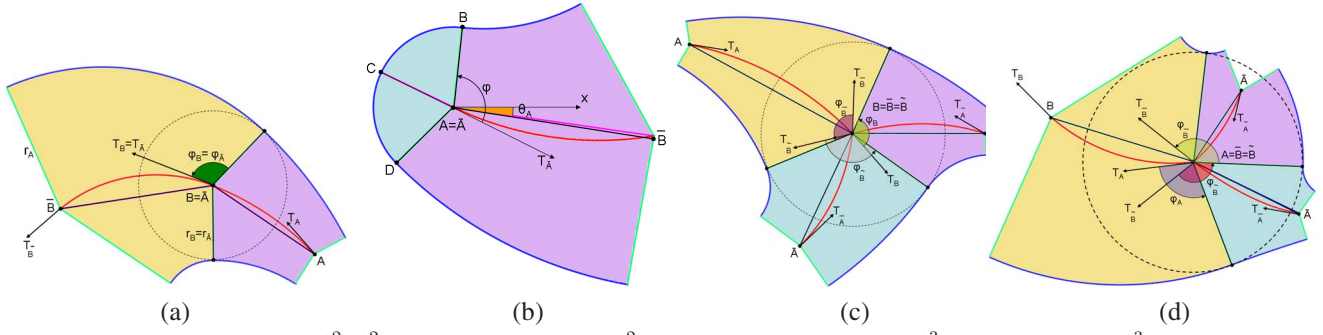


Figure 8. Constraints at (a)  $A_1^2$ - $A_1^2$  fragment interface, (b)  $A_1^2$ - $A_\infty$  fragment interface, (c)  $A_1^3$  - 4 node, and (d)  $A_1^3$  - 2 node.

**node):** Let the three fragments

$$\chi_{AB} = \{(x_A, y_A, \theta_A, \lambda_A), (\phi_A, \phi_B, m_A), \eta_A\}$$

$$\chi_{\overline{AB}} = \{(x_{\overline{A}}, y_{\overline{A}}, \theta_{\overline{A}}, \lambda_{\overline{A}}), (\phi_{\overline{A}}, \phi_{\overline{B}}, m_{\overline{A}}), \eta_{\overline{A}}\}$$

$$\chi_{\overline{A}\overline{B}} = \{(x_{\overline{A}}, y_{\overline{A}}, \theta_{\overline{A}}, \lambda_{\overline{A}}), (\phi_{\overline{A}}, \phi_{\overline{B}}, m_{\overline{A}}), \eta_{\overline{A}}\}$$

come together at an  $A_1^3$  - 4 node. Then we have nine constraints, Figure 8(c): (i)  $x_B = x_{\overline{B}} = x_{\overline{B}}$ , (ii)  $y_B = y_{\overline{B}} = y_{\overline{B}}$ , (iii)  $r_B = r_{\overline{B}} = r_{\overline{B}}$ , (iv)  $\theta_B + \alpha_B + \phi_B = \theta_{\overline{B}} + \alpha_{\overline{B}} - \phi_{\overline{B}}$ , (v)  $\theta_{\overline{B}} + \alpha_{\overline{B}} + \phi_{\overline{B}} = \theta_{\overline{B}} + \alpha_{\overline{B}} - \phi_{\overline{B}}$ , and (vi)  $\theta_{\overline{B}} + \alpha_{\overline{B}} + \phi_{\overline{B}} = \theta_B + \alpha_B - \phi_B$ . Thus, three  $A_1^3$  fragments coming together at an  $A_1^3$  - 4 node have  $8 + 8 + 8 - 9 = 15$  degrees of freedom.

IV.  $A_1^3$  - 2 fragments (three  $A_1^2$  fragments at  $A_1^3$  - 2 nodes): Let the three fragments

$$\chi_{AB} = \{(x_A, y_A, \theta_A, \lambda_A), (\phi_A, \phi_B, m_A), \eta_A\}$$

$$\chi_{\overline{AB}} = \{(x_{\overline{A}}, y_{\overline{A}}, \theta_{\overline{A}}, \lambda_{\overline{A}}), (\phi_{\overline{A}}, \phi_{\overline{B}}, m_{\overline{A}}), \eta_{\overline{A}}\}$$

$$\chi_{\overline{A}\overline{B}} = \{(x_{\overline{A}}, y_{\overline{A}}, \theta_{\overline{A}}, \lambda_{\overline{A}}), (\phi_{\overline{A}}, \phi_{\overline{B}}, m_{\overline{A}}), \eta_{\overline{A}}\}$$

come together at an  $A_1^3$  - 2 point. Then we have nine constraints, Figure 8(d): (i)  $x_A = x_{\overline{B}} = x_{\overline{B}}$ , (ii)  $y_A = y_{\overline{B}} = y_{\overline{B}}$ , (iii)  $r_A = r_{\overline{B}} = r_{\overline{B}}$ , (iv)  $\theta_A + \alpha_A - \phi_A = \theta_{\overline{B}} + \alpha_{\overline{B}} - \phi_{\overline{B}}$ , (iv)  $\theta_{\overline{B}} + \alpha_{\overline{B}} + \phi_{\overline{B}} = \theta_{\overline{B}} + \alpha_{\overline{B}} - \phi_{\overline{B}}$ , and (iv)  $\theta_{\overline{B}} + \alpha_{\overline{B}} + \phi_{\overline{B}} = \theta_A + \alpha_A + \phi_A$ . Thus, three  $A_1^3$  fragments coming together at an  $A_1^3$  - 2 node have  $8 + 8 + 8 - 9 = 15$  degrees of freedom.

## 5. Shapes from Fragments: Putting It All together

The previous sections addressed the questions of representing individual shock fragments and the constraints arising from adjacent fragments, which significantly reduce the number of free variables for adjacent matching fragments. The following proposition shows that the number of free variables is linearly dependent on the number of edges and end-points for any shock graph:

**Proposition 5. (Degrees of freedom of a shock graph)** Let  $(G)$  be a directed tree representing a shock graph topology whose nodes have degree 1, 2, or 3. Let  $M$  be the total

number of edges and  $N_i$  be the total number of degree- $i$  nodes in  $G$ . Then the degree of freedom of PCAS contours giving rise to this shock graph is  $3M + N_1 + 3$ .

The above proposition illustrates that the number of free parameters for any given shock graph is not unwieldy, but it does not highlight which set of variables can or should be chosen overall as a set of free variables. While in theory any set of independent variables will do, some will lead to more complicated equations, *e.g.*, for boundary reconstruction. As an example, while the extrinsic variables for each node can be treated as independent variables, that would leave the notion of shape, which is invariant to translation and rotation, implicit in the representation. On the other hand, treating the extrinsic coordinates as dependent variables brings out this notion. Thus, one set of location and orientation  $(x_0, y_0, \theta_0)$  can be free and all other extrinsic parameters can be treated as dependent.

**Proposition 6. (Shock graph parameter set)** Let  $G$  be a shock graph,  $G = (V, E)$ , where  $V$  is the vertex set and  $E$  is the edge set,

$$\begin{aligned} V &= \{v_1, v_2, \dots, v_N\} \\ E &= \{e_1, e_2, \dots, e_M\}. \end{aligned} \quad (4)$$

Let  $\Phi_k = \{\phi_1^k, \phi_2^k, \dots, \phi_{p-1}^k\}$  be the set of  $(p-1)$  (out of the total of  $p$ ) angle  $\phi_j$ 's associated with each vertex  $v_k$  of degree  $d$ , where  $p = d$  for  $d > 1$  and  $p = 2$  for  $d = 1$ . Let  $L_i$  be the distance between the two nodes of the edge  $e_i$ . Let  $(x_0, y_0)$  and  $r_0$  be the coordinates and radius of some node, say  $v_1$ , and  $\theta_0$  the direction of the chord of some edge at that node, say  $e_1$ . Then, the set of variables

$$\begin{aligned} S &= \{(\Phi_1, \Phi_2, \dots, \Phi_N), \\ &\quad (m_1, m_2, \dots, m_M), \\ &\quad (L_1, L_2, \dots, L_M), \\ &\quad (x_0, y_0, \theta_0), r_0\} \end{aligned} \quad (5)$$

fully specifies a PCAS which is free of intersection and has the shock graph topology  $G$  as specified, Figure 9.

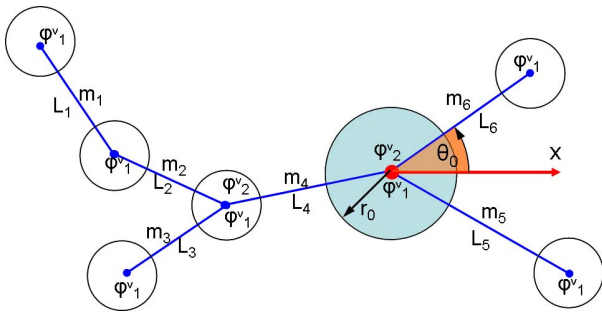


Figure 9. The independent parameter set for a PCAS is distributed across the vertices and edges: 2 parameters ( $m_i, L_i$ ) per edge  $e_i$  and  $(p - 1)$  parameters ( $\phi_1^k, \phi_2^k, \dots, \phi_{p-1}^k$ ) per degree- $d$  vertex  $v_k$ , where  $p = d$  for  $d > 1$  and  $p = 2$  for  $d = 1$ . Additional to these intrinsic parameters are the extrinsic parameters  $(x_0, y_0, \theta_0)$  specifying the location and orientation of the graph and a reference radius  $r_0$  for one vertex.

## 6. Experiments

The focal point of this paper is to present a generative model of shapes and theoretically derive a complete, relatively low-dimensional model for free-form shape approximated to the desired degree. The experiments presented below (a) generate neighboring shapes of the same skeletal graph to any generic shapes, (b) use in morphing shapes, and (c) indicate the potential of using it as a deformable model. While the true test of the theory requires additional development to enable the use of this generative model in the four application areas described earlier and proper validation in each area, we hope that the experiments illustrate the potential of the presented theory.

(a) The parameter set (5) allows us to generate all shapes given a shock graph topology. Conversely, if we have shape instance, we can find out its skeletal topology and the parameters associated with that specific instance by (i) approximate its boundary with circular arcs, then (ii) compute its shock graph, Figure 10. We then generate its neighboring shapes with the same skeletal graph by varying its parameters in a continuous fashion, Figure 11.

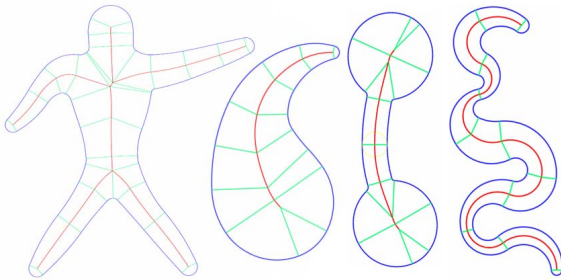


Figure 10. Examples of symmetry-base models constructed automatically for various shapes.

(b) Morphing a shape into another based on a contour-based representation can lead to illegal intermediate shapes. Cur-

rently symmetry-based morphing is mostly restricted between shapes of the same skeletal topology [16]. We use the geodesic path indicating what changes the shock graph of our shape must undergo to become the shock graph of a second shape [21]. We then use our generative model to put “flesh” on this skeletal transitions, by linearly interpolate its parameter set, Figure 12.

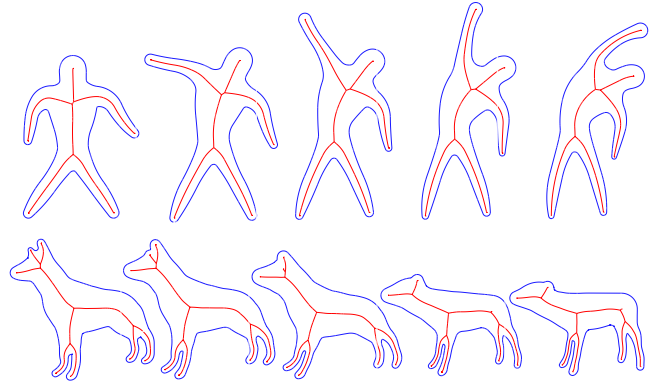


Figure 12. Application of a morphing between two shapes using our model. (Top row) Morphing between two shapes with the same skeleton topology is generated in a fully automated fashion. (Bottom row) Morphing between two shapes with different topology skeleton using our proposed model. This sequence is guided by the edit distance path described in [21].

(c) We construct a simple deformable model using our approach by starting with a simple “seed” shape and adjusting the topology of the graph as the image forces deform the boundary of the shape. Our examples in this paper are restricted to “axial growth” but the approach is general. Specifically, the model is initialized with a “seed fragment” that fits well to the image. In each iteration, two new fragments are added to one end of the graph to capture a new portion of the object by optimizing their parameters with respect to a snake-like energy functional. The process is repeated till each side of the graph hits a predetermined point given by the user. Figure 13 (a) shows the result of segmenting the “S” shape from a synthetic image while Figure 13 (b) shows the segmentation of the knee cartilage from an MRI image using this model.

## References

- [1] M. Alexa, D. Cohen-Or, and D. Levin. As-rigid-as-possible shape interpolation. In *SIGGRAPH* 2000.
- [2] A. O. Balan and M. J. Black. An adaptive appearance model approach for model-based articulated object tracking. In *CVPR* 2006.
- [3] S. Belongie, J. Malik, and J. Puzicha. Shape matching and object recognition using shape contexts. *PAMI* 2002.
- [4] S. Bischoff and L. P. Kobbelt. Parameterization-free active contour models with topology control. *Vis. Comput.* 2004.

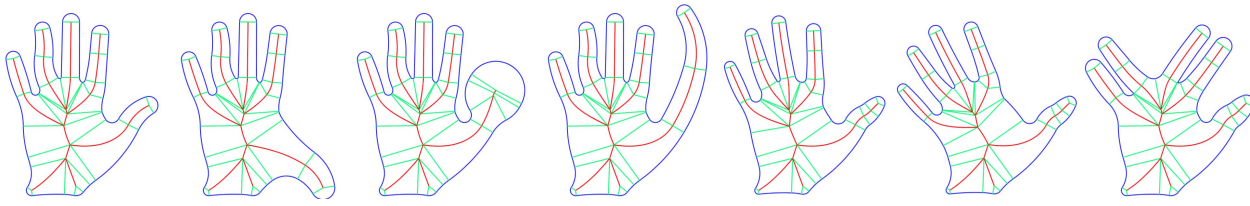


Figure 11. Our approach provides a low-dimensional representation for generating and deforming shapes given a shock graph topology. In this example, the given graph implies a 58-dimensional space that generates all possible shapes from piecewise circular boundaries, 7 of which are shown here. Adding a shape prior will further constrains the space of variation.

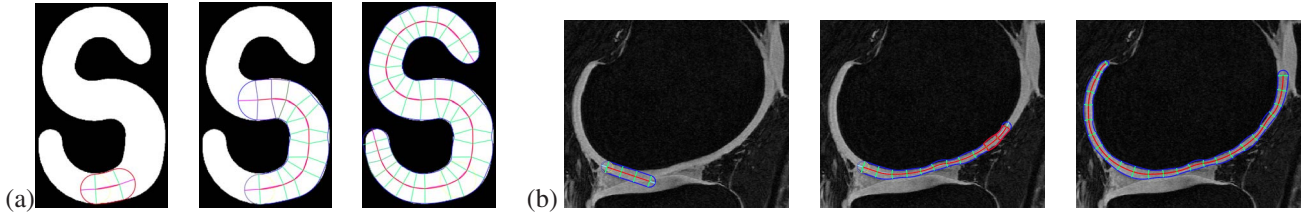


Figure 13. Application of a one-branch symmetry-based deformable model to segment (a) the “S” shape from a synthetic image, and (b) knee cartilage from an MRI image. Initialized with a simple bar shape placed inside the object of interest the model extends itself on one side with two fragments and optimized the two new fragments to match with the edges of the underlying image. The process is repeated until the model hits the end of the object. It then repeats the procedure for the other side of the initial bar shape.

[5] F. Bookstein. Landmark methods for forms without landmarks: morphometrics of group differences in outline shape. *MIA* 1996/7.

[6] T. Cootes, C. Taylor, D. Cooper, and J. Graham. Active shape models - their training and applications. *CVIU* 1995.

[7] D. Cremers, S. Osher, and S. Soatto. Kernel density estimation and intrinsic alignment for shape priors in level set segmentation. *IJCV* 2006.

[8] P. J. Giblin and B. B. Kimia. On the intrinsic reconstruction of shape from its symmetries. *PAMI* 2003.

[9] J. Glaunes, A. Trouvé, and L. Younes. Diffeomorphic matching of distributions: A new approach for unlabelled pointsets and sub-manifolds matching. In *CVPR* 2004.

[10] X. Han, C. Xu, and J. L. Prince. A topology preserving level set method for geometric deformable models. *PAMI* 2003.

[11] T. Igarashi, T. Moscovich, and J. F. Hughes. As-rigid-as-possible shape manipulation. *ACM Trans. Graph.* 2005.

[12] A. Jain, Y. Zhong, and S. Lakshmanan. Object matching using deformable templates. *PAMI* 1996.

[13] S. Joshi, S. Pizer, P. Fletcher, P. Yushkevich, A. Thall, and J. Marron. Multiscale deformable model segmentation and statistical shape analysis using medial descriptions. *TMI* 2002.

[14] M. Kass, A. Witkin, and D. Terzopoulos. Snakes: active contour models. *IJCV* 1988.

[15] M. E. Leventon, W. E. L. Grimson, and O. D. Faugeras. Statistical shape influence in geodesic active contours. In *CVPR* 2000.

[16] J. P. Lewis, M. Cordner, and N. Fong. Pose space deformation: a unified approach to shape interpolation and skeleton-driven deformation. In *SIGGRAPH* 2000.

[17] R. Malladi, J. A. Sethian, and B. C. Vemuri. Shape modelling with front propagation: A level set approach. *PAMI* 1995.

[18] J. Mundy and A. Zisserman. Geometric invariance in computer vision. *MIT Press, Cambridge, USA*, 1992.

[19] A. Pentland, I. Essa, M. Friedmann, B. Horowitz, and S. E. Scharoff. The thingworld modeling system: virtual sculpting by modal forces. *SIGGRAPH* 1990.

[20] S. M. Pizer, P. T. Fletcher, S. Joshi, A. Thall, J. Z. Chen, Y. Fridman, D. S. Fritsch, A. G. Gash, J. M. Glotzer, M. R. Jiroutek, C. Lu, K. E. Muller, G. Tracton, P. Yushkevich, and E. L. Chaney. Deformable m-reps for 3d medical image segmentation. *IJCV* 2003.

[21] T. Sebastian, P. Klein, and B. Kimia. Recognition of shapes by editing their shock graphs. *PAMI* 2004.

[22] L. Staib and J. Duncan. Boundary finding with parametrically deformable models. *PAMI* 1992.

[23] D. Terzopoulos and D. N. Metaxas. Dynamic 3D models with local and global deformations: Deformable superquadrics. *PAMI* 1991.

[24] J. Triesch and C. von der Malsburg. Classification of hand postures against complex backgrounds using elastic graph matching. *IVC* 2002.

[25] X. Yang. Efficient circular arc interpolation based on active tolerance control. *Computer-Aided Design* 2002.

[26] A. L. Yuille, P. W. Hallinan, and D. S. Cohen. Feature extraction from faces using deformable templates. *IJCV* 1992.

[27] P. Yushkevich, P. T. Fletcher, S. Joshi, A. Thall, and S. M. Pizer. Continuous medial representations for geometric object modeling in 2d and 3d. *IVC* 2003.

[28] P. A. Yushkevich, H. Zhang, and J. C. Gee. Parametric medial shape representation in 3-d via the poisson partial differential equation with non-linear boundary conditions. In *IPMI* 2005.

[29] J. Zhang, R. T. Collins, and Y. Liu. Representation and matching of articulated shapes. In *CVPR* 2004.